Journal of Nonlinear Optical Physics & Materials
Vol. 33, No. 3 (2024) 2350042 (19 pages)

DOI: 10.1142/S021886352350042X

World Scientific
www.worldscientific.com

Flat-top and broadband supercontinuum generation in CCl_4-filled circular photonic crystal fiber

Thuy Nguyen Thi*,‡, Duc Hoang Trong*, Bao Tran Le Tran† and Lanh Chu Van†,§

*University of Education, Hue University, 34 Le Loi Street
Hue City, Vietnam

†Department of Physics, Vinh University, 182 Le Duan
Vinh City, Vietnam
‡ntthuy@hue.uni.edu.vn
§chuvanlanh@vinhuni.edu.vn

Received 7 April 2022
Revised 11 November 2022
Accepted 14 November 2022
Published 25 January 2023

In this work, a flat-top and broadband supercontinuum (SC) generation in photonic crystal fibers (PCFs) infiltrated with carbon tetrachloride (CCl_4) with different air hole diameters in the cladding has been introduced. The optical properties of the fundamental mode are analyzed by numerical simulation. Based on the obtained results, two optimized PCFs with small dispersion are proposed and verified against SC generation in detail. The first fiber has an all-normal dispersion of $-9.376\,\mathrm{ps.nm^{-1}.km^{-1}}$ at the pump wavelength of $0.98\,\mu$m, generating broadband of 768 nm and flat-top with only 0.3 nJ of input energy and time duration of 90 fs. In the meantime the dispersion property of the second fiber is anomalous, which equals $1.105\,\mathrm{ps\cdot nm^{-1}\cdot km^{-1}}$ at $1.3\,\mu$m pump wavelength. The second fiber generates a SC spectrum of 1,751.1 nm with input energy and time duration of 0.55 nJ and 55 fs, respectively. Proposed fibers are suitable for all-fiber SC sources which could lead to new low-cost all-fiber optical systems.

Keywords: PCF; carbon tetrachloride infiltration; supercontinuum generation; flat-top supercontinuum generation; all-normal dispersion; anomalous dispersion.

1. Introduction

Supercontinuum (SC) generation has been one of the most active fields of research during the last decades thanks to its diverse applications such as spectroscopy, optical microscopy, optical communication, telecommunication, security, military, optical coherent tomography, biomedicine, frequency comb generation, and nonlinear optical pulse compression.[1–12] The flexibility in the structural design, the controllability of the dispersion and interesting nonlinear properties make photonic crystal fiber (PCF) naturally attractive for SC generation. The spectral width and

‡Corresponding author.

flatness over broadband wavelength have been two essential factors in evaluating the effectiveness of SC generation. Up to now, obtaining a relatively broad and flat spectrum has been a challenge for many research groups. This makes the study of PCFs with optimal dispersion and nonlinear properties more attractive than ever, both theoretically and experimentally. Selection of the appropriate base material along with the modification of the structure parameters in the cladding or the shape of lattice geometry provides high efficiency in controlling the dispersion, transmission, and even the nonlinear properties of PCF.[13–17] In which, PCFs infiltrations with liquids is one of the most excellent solutions to achieve optimal dispersion, especially suitable for generating SC due to the relatively high nonlinear refractive indices of liquids when compared to solids (up to 100 times larger compared to fused silica[18]). Another advantage is that some highly nonlinear liquids are transparent in the visible and near-infrared (IR) wavelength range,[19] which is necessary for the SC to broaden further in this spectral region. The highly nonlinear properties of the fluids allow for a decrease in the required powers significantly, which makes liquid-filled fibers also available for cheap, and compact pump lasers.[20] However, a high toxicity as well as explosive, carcinogenic, and volatile properties[21] are factors that should be kept in mind. Except for carbon disulfide, using liquids such as chloroform, carbon tetrachloride (CCl_4), tetrachloroethylene, nitrobenzene, benzene, and toluene has been preferred in real applications.

It is well known that the dispersion characteristic of the optical fiber is an important factor governing the SC generation process.[22] Diverse studies of liquid-core PCFs show the ability to control dispersion as well as to shift the zero-dispersion wavelengths (ZDWs), and match it with the pump wavelength of commercial lasers to obtain flat, coherent, and broadband SC generation. The all-normal and anomalous flat dispersion with one or two ZDWs have been found in these liquid core PCFs. The self-phase modulation (SPM), self-steepening (SS), and optical wave breaking (OWB) are the main nonlinear effects that dominate the spectral broadening of output optical pulses when a nonlinear medium is pumped in the normal dispersion region, which easily generates a smooth, flat, and coherent spectrum. If PCF is pumped in the anomalous dispersion regime, the soliton dynamics, e.g., soliton fission (SF), soliton self-frequency shift (SSFS), and dispersive wave (DW) will be the main contributors to SC generation. In this case, the spectrum is broader but less coherent.[23–26]

Many studies used liquids with high nonlinear refractive index to partially replace the air holes or fill the hollow cores of PCFs. These methods show their potential in further improving dispersion and achieving other interesting nonlinear properties. The all-normal and anomalous dispersion characteristics were found in PCF filled with chloroform, the authors of Ref. 27 have proved the possibility of coherent octave-wide SC generation but rather high dispersion values at pump wavelength limit further spectral expansion. At the same time, the input pulses injected into the fiber have quite high energy and time duration. Using a combination of fluids such as arsenic-selenide and chloroform, which are infiltrated into air holes in different rings

of the cladding, PCFs[28] give an ultra-wideband SC spectra up to 19 μm but the short propagation length of the fiber and the toxicity of the used liquid are also factors that need attention in the real application. Diversity in dispersion gives the authors many options in studying SC generation using optimal structures, which is a common advantage of PCFs filled with liquids such as benzene,[29] nitrobenzene,[30,31] tetrachlorethylene,[32] toluene.[33–35] Usually, the variation of the structural parameters of these fibers also helps to control both all-normal and anomalous dispersions well, which is beneficial for broad-spectrum SC generation. However, some fibers have a bit short propagation length[30] or the nonlinear characteristics are not optimized simultaneously or the input pulse energy is quite high,[32–35] which has a significant influence on the efficiency of SC generation.

CCl_4 is one of the most interesting liquids used to fill hollow core PCF due to a very high nonlinear refractive index, $n_2 = 1.53 \times 10^{-19}\,\mathrm{m^2/W}$ at $\lambda = 1.064\mu\mathrm{m}$[18] (up to 5 times larger compared to fused silica (SiO_2) $n_2 = 2.74 \times 10^{-20}\,\mathrm{m^2/W}$) and low toxicity when compared to other liquids such as carbon disulfide or toluene.[21] Optimization of dispersion and nonlinear properties of PCFs infiltrated with CCl_4 for SC generation have been studied both theoretically and experimentally. By infiltrating CCl_4 into the hollow core, most of the PCFs in the papers[36–39] give all-normal dispersion. The paper[36] proved the possibility of coherent, octave-spanning SC generation with 300 fs pulses with only 0.8 nJ of input energy of PCF made of fused silica glass, infiltrated with CCl_4. A large hollow core PCF infiltrated with CCl_4 to generate SC with all-normal dispersion was studied experimentally in the work.[37] A flat normal dispersion in a broadband range (0.8–1.7 μm) varying from -150 to 0 ps/nm/km meets the requirements for an all-fiber SC system despite the large effective mode area of 42.2 $\mu\mathrm{m}^2$ at the pump wavelength ($\lambda = 1030$ nm). An all-normal SC in the 850–1,250 nm wavelength range was generated using an off-the-shelf 1,030 nm fiber laser with 400 fs and 25 nJ input pulses. The SC spectrum spanning from 1,000 nm to 1,900 nm in CCl_4-filled hollow-core PCF under pumping with a small-footprint femtosecond laser with a central wavelength at 1,560 nm and a pulse duration of 90 fs was also investigated experimentally.[38] Another study of solid-core PCF with cladding air-holes infiltrated with CCl_4 using bismuth lead-bismuth-gallate glass was also experimentally investigated and numerically verified. The unique combination of high nonlinearity and low normal dispersion of PCFs enables the generation of a coherent, low-noise SC covering 0.93–2.5 μm requiring only 12.5 kW of pump peak power delivered by a standard ultrafast erbium-fiber laser with 100 MHz pulse repetition rate.[39]

Although these publications demonstrate the ability to generate a coherent and broad SC spectrum of PCFs infiltrated with CCl_4 thanks to the control of dispersion properties, a quite large effective mode area, low nonlinear coefficient, and high loss were also observed. Furthermore, the flat-top and smooth SC spectrum in an all-normal dispersion regime with small input pulse energy have not been mentioned. It should be noted that we find it very difficult to optimize the characteristic quantities of PCF simultaneously, depending on the structural design and the selection of an

appropriate substrate or alternative material to obtain the optical properties of the PCF as expected.

In this work, we design a circular lattice PCF, the hollow-core is filled with CCl_4. To control dispersion and optimize nonlinear properties, the diameter of the air holes of the first ring near the core in the cladding is different from that of the other rings. The high symmetry of the circular lattice can confine the light more strongly to the core than other lattices, which enhances the PCF nonlinearity, and improves the SC generation efficiency. We demonstrate the ability to achieve both all-normal and anomalous dispersions with a small value of -9.376 and 1.015 ps/nm/km, respectively, small effective mode area, and low loss of the fundamental mode at the pumping wavelength. Based on the analysis results, SC generation has been investigated numerically through two optimal dispersion fibers. For all-normal dispersion, the output pulse is broadened from 609.4 to 1,377.4 nm requiring only 0.3 nJ input energy and time duration of 90 fs with a flat-top and smooth spectrum. The fiber with anomalous dispersion generates a high-quality SC with spectral bandwidth covering 733.3–2484.4 nm with input energy of 0.55 nJ and time duration of 0.55 fs.

2. Numerical Modeling of the PCFs

Eight rings of air holes were distributed in a circular structure around the hollow-core filled with CCl_4 of PCF based on fused silica material, depicted in Fig. 1(a). A combination of both, including selecting an appropriate liquid to replace the solid core, and carefully modifying significant structural parameters, was used to design these PCs. Several studies[13,35,40,41] have shown that dispersion properties of PCFs including ZDWs shifts are fundamentally affected by the size (the diameter of d_1) of innermost air holes of the cladding while the diameter d_2 of others is usually adjusted to reduce the attenuation of the fundamental mode and even the higher modes. Here, we have designed the PCFs for values of filling factor d_1/Λ (Λ is the lattice constant) tailoring from 0.3 to 0.8 with a step of 0.5 μm and $\Lambda = 1.0, 2.0\,\mu$m but the value of d_2/Λ is kept constant at 0.95 to present diverse dispersion properties in all-normal

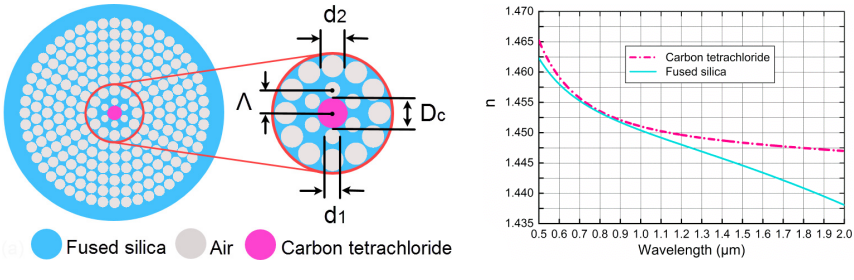

(a) (b)

Fig. 1. Cross-section view of the circular CCl_4-PCF (a) and the real parts of the refractive index n of CCl_4 and fused silica (b).

and anomalous regimes. The combination of small core size to wavelength ratio and difference in refractive indices between core and cladding are key factors to be kept in mind when designing to achieve a single-mode PCF. So, the small core of the PCF has a diameter determined by the formula $D_c = 2\Lambda–1.2d_1$. The small core also enhances the ability to confine light inside the core and is more convenient in fiber fabrication. These designs allow the generation of flat-top SC over a wide wavelength range.

The real parts of the refractive index n of CCl_4 and fused silica used in this paper versus wavelength are shown in Fig. 1(b). Interestingly, the linear refractive index of CCl_4 is low and similar to fused silica, which enables CCl_4-filled PCF to achieve high coupling efficiency with typical silica fibers used in all-fiber pump laser systems.[42,43] Moreover, the small difference between the linear refractive index of CCl_4 and the fused silica is also one of the favorable conditions for the formation of a single-mode fiber that helps the electromagnetic field energy to concentrate on the core, i.e., enhances the nonlinearity of optical fiber. The dependence of refractive index characteristics on wavelength for CCl_4 and fused silica is described by Cauchy's equation[44] and Sellmeier's equation[45]:

$$n^2_{CCl_4}(\lambda) = 2.085608282 + 0.00053373\lambda^2 + \frac{0.012201206}{\lambda^2} + \frac{0.000056451}{\lambda^4} + \frac{0.000048106}{\lambda^6}, \tag{1}$$

$$n^2_{SiO_2}(\lambda) = 1 + \frac{0.6961663\lambda^2}{\lambda^2 - (0.0684043)^2} + \frac{0.4079426\lambda^2}{\lambda^2 - (0.1162414)^2} + \frac{0.8974794\lambda^2}{\lambda^2 - (9.896161)^2}, \tag{2}$$

where λ is the excitation wavelength in micrometers, $n(\lambda)$ is the wavelength-dependent linear refractive index of materials.

There are many numerical simulation methods to achieve the field intensity profile of the fundamental mode of PCFs, the full-vector finite-difference eigenmode (FDE) method is very popular to calculate the efficiency of refractive indices of micro-structured holey fibers. We use this method to analyze the light propagation characteristics of PCFs through lumerical mode solutions (LMSs) software. The simulation is limited for the wavelength range of 0.6–2.0 μm because the reliable data are available only in this range. The simulation is performed with the assumption that CCl_4 exhibits significant losses. The process of FDE utilizes the Maxwell wave equation and the boundary condition for simulation is a perfectly matched layer, allowing no reflection at the boundary and reducing the loss.

3. Optical Properties of the PCFs

The higher order modes have no significant effect on the SC broadening if the input pulse is sufficiently short (≤ 10 ps),[46] so here we only present the fundamental mode dispersion. The chromatic dispersion (D) of a PCF including both the

material dispersion and the waveguide dispersion can be defined using the following equation[47]:

$$D = -\frac{\lambda}{c}\frac{\partial^2 \mathrm{Re}[n_{\mathrm{eff}}]}{\partial \lambda^2}, \tag{3}$$

where λ and c are the wavelength and the speed of light in vacuum, respectively, and $\mathrm{Re}[n_{\mathrm{eff}}]$ is the real part of the effective index of the guided mode.

The effective mode area is an important parameter in designing PCFs. It measures how much the mode field is confined within the PCF core, which can be computed using[48]

$$A_{\mathrm{eff}} = \frac{\left(\int_{-\infty}^{\infty}\int_{-\infty}^{\infty}|E|^2 dxdy\right)^2}{\int_{-\infty}^{\infty}\int_{-\infty}^{\infty}|E|^4 dxdy}, \tag{4}$$

where E denotes the amplitude of the transverse electric field propagating inside the PCF.

The Kerr nonlinearity coefficient γ is expressed as[49]:

$$\gamma(\lambda) = 2\pi\frac{n_2}{\lambda A_{\mathrm{eff}}} \tag{5}$$

with n_2 is the nonlinear refractive index for fused silica.

Confinement loss (L_c) can be derived from the imaginary part of the effective refractive index $\mathrm{Im}[n_{\mathrm{eff}}(\lambda)]$ of the PCF by[50]

$$L_c = 8.686\frac{2\pi}{\lambda}\mathrm{Im}[n_{\mathrm{eff}}(\lambda)]. \tag{6}$$

The chromatic dispersion depends strongly on the wavelength, the value of the filling factor d_1/Λ, and lattice constant Λ, displayed in Fig. 2. It is clear to observe that the CCl_4-PCFs exhibits both all-normal and anomalous dispersions with one or

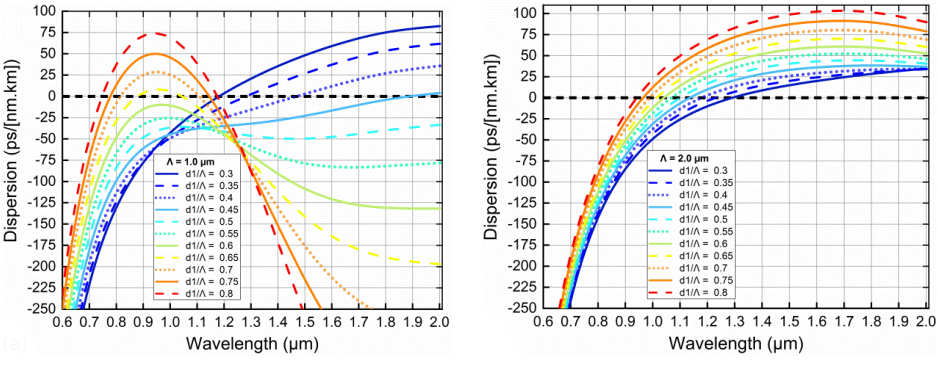

(a) (b)

Fig. 2. The chromatic dispersion characteristics of CCl_4-PCFs with various values of d_1/Λ and $\Lambda = 1.0\,\mu$m (a); $2.0\,\mu$m (b).

two ZDWs for smaller core PCFs, $\Lambda = 1.0\,\mu$m (Fig. 2(a)). More, the left part of the dispersion curve shifts towards shorter wavelengths as d_1/Λ increases. When d_1/Λ is smaller than 0.45, the dispersion curve lies in anomalous dispersion regime with one ZDW and it shifts towards an anomalous dispersion regime with double ZDWs on increasing the value of d_1/Λ (0.65–0.8). In the other case, the overall dispersion curve falls in all-normal region, increasing the values of the filling factor d_1/Λ (0.5–0.6) makes the all-normal dispersions flatter and closer to the zero dispersion line which is expected to be beneficial for SC generation. The interaction between waveguide dispersion and material dispersion may be responsible for the dispersion diversity in the case of small cores. Matter dispersion prevails for smaller d_1/Λ while the waveguide effect plays a major role for higher d_1/Λ. For $\Lambda = 2.0\,\mu$m (Fig. 2(b)), a huge change in the nature of dispersion profile of larger core PCFs has been observed, anomalous dispersion regime with one ZDW dominates completely in the investigated wavelength range and ZDWs move to shorter wavelength side. The flattest and closest curve to the zero-dispersion is $d_1/\Lambda = 0.7$. The above analysis and simulated results show that it seems easy to get desirable dispersion characteristic of the structure by carefully tuning air hole diameter d_1 in the first ring of PCF structure.

The variation of propagation of optical pulses per unit distance of propagation length of the fiber results from the interplay between dispersive and nonlinear processes in PCF. It is well known that flat and near-zero dispersion is highly demanded for efficient SC generation.[34] Besides, the pumping wavelength, pulse duration, peak power, and length of the fiber are also the determining factors for the generation of a broadband SC. Based on the preliminary analysis of the dispersion, we propose two PCFs with suitable dispersion to study in detail the SC generation, named $\#F_1$ and $\#F_2$. Compared to the other fibers, their dispersion appears flatter and closer to zero dispersion. The chromatic dispersion characteristics of the fundamental mode for $\#F_1$ and $\#F_2$ fibers are illustrated in Fig. 3. With an all-normal dispersion regime and closest to zero dispersion, fiber $\#F_1$ ($\Lambda = 1.0\,\mu$m, and $d_1/\Lambda = 0.6$) is expected to generate flat-, smooth-, and broad-spectrum SC at the pump wavelength of $0.98\,\mu$m. For $\Lambda = 2.0\,\mu$m, and $d_1/\Lambda = 0.3$, $\#F_2$ exhibited an anomalous dispersion characteristic, used as a nonlinear medium for SC generation with the pumping wavelength of $1.3\,\mu$m. This wavelength is very close to ZDW of $\#F_2$ fiber, which is $1.29\,\mu$m. The values of dispersion at the pump wavelength for both $\#F_1$ and $\#F_2$ are –9.376 and $1.015\,\text{ps.nm}^{-1}.\text{km}^{-1}$, respectively. Low anomalous dispersion near the ZDW of $\#F_2$ fiber provides the generation of a broad SC with strong confinement to the core.[20]

When the ultrashort pulse propagates along the fiber, it interacts with the nonlinear optical medium and generates new frequencies through various nonlinear effects resulting in SC spectrum broadening. So, the nonlinear properties of optical fibers play a key role in enhancing the SC efficiency. Light is better confined in the core of the PCF due to a large index contrast between the core and cladding, which allows the nonlinear coefficients to be improved as expected. Both the effective mode area and the nonlinear coefficient of $\#F_1$ and $\#F_2$ fiber have been computed and illustrated in Figs. 4 and 5, respectively. The effective mode area values of the two

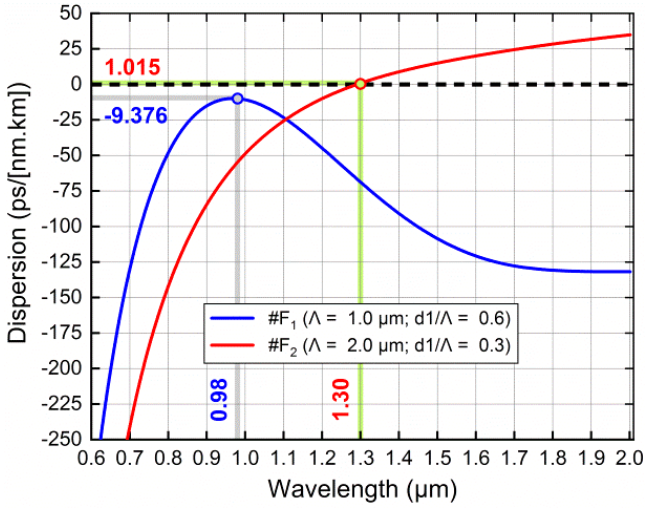

Fig. 3. The chromatic dispersion characteristics of the fundamental mode for $\#F_1$ and $\#F_2$ fibers.

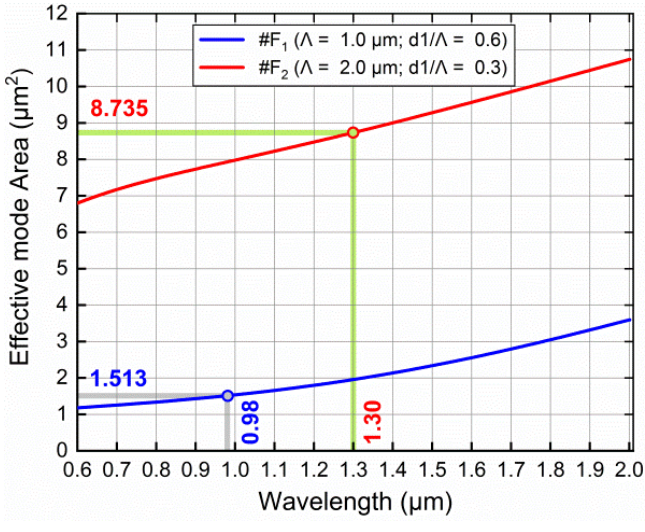

Fig. 4. The effective mode area of the fundamental mode for $\#F_1$ and $\#F_2$ fibers.

fibers are calculated as 1.513, and 8.735 μm^2 at the pump wavelength, respectively, these values are relatively small in comparison with previous publications of PCF with various highly nonlinear liquids.[32,34,36,37] The effective mode area of the proposed fibers rises up along with increasing wavelength, because of the leakage of modes through the holes. Ordinarily, a smaller core leads to a smaller effective mode area, and thus the nonlinear coefficient associated with effective mode area will increase because light concentrates more on the small core of the CCl_4 fibers, so $\#F_2$

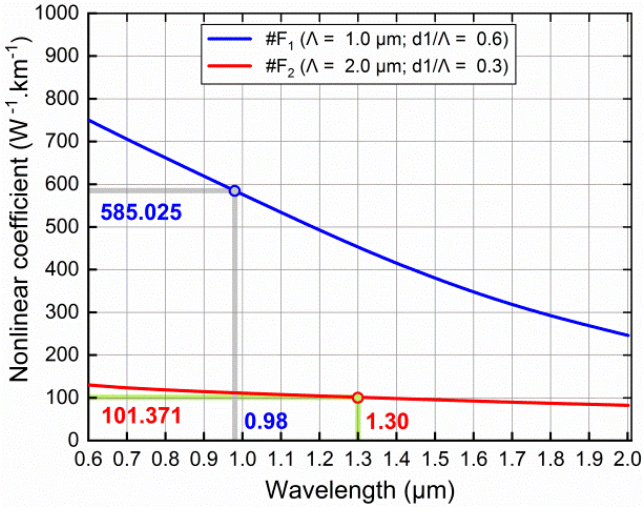

Fig. 5. The nonlinear coefficient of the fundamental mode for $\#F_1$ and $\#F_2$ fibers.

fiber has a larger effective mode area than that of $\#F_1$. Using these effective mode area values, the relatively high nonlinear coefficients γ can be computed as 101.371 and 585.025 $W^{-1}.km^{-1}$, respectively. More, varying the different structures parameters of the PCF has also allowed the optimization of the confinement loss, its relationship with the wavelength of the fundamental mode is displayed in Fig. 6. The confinement loss increases with the increase of wavelength which occurs due to the leakage of the modes of the optical fiber. The relatively low confinement loss indicates a large amount of well-confined fundamental mode in the core region, therefore,

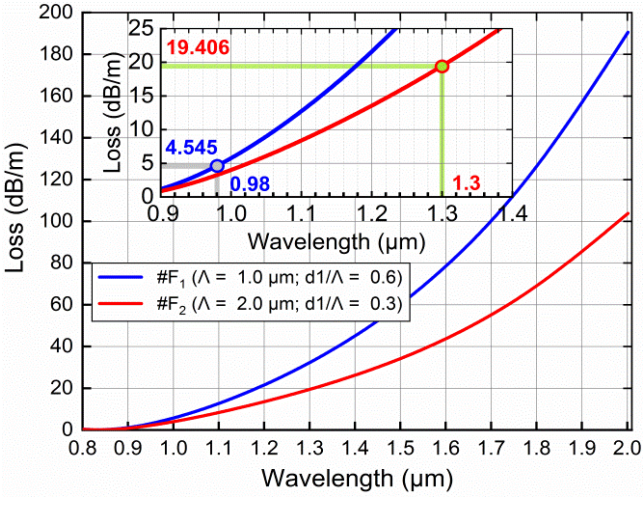

Fig. 6. The confinement loss of the fundamental mode for $\#F_1$ and $\#F_2$ fibers.

Table 1. The structure parameters and the characteristic quantities of proposed PCFs at the pump wavelength in comparison with some previous work on liquid-filled PCFs.

#	Refs.	Λ (μm)	d_1/Λ	Pump wavelength (μm)	D (ps/nm.km)	A_{eff} (μm^2)	γ (km^{-1}.W^{-1})	L_c (dB/m)
$\#F_1$	This work	1.0	0.6	0.98	−9.376	1.513	585.025	4.545
$\#F_2$	This work	2.0	0.3	1.3	1.015	8.735	101.371	19.406
$CHCl_3$, $\#F_1$	27	1.0	0.65	0.92	−24.0	1.5	1290	—
$CHCl_3$, $\#F_2$	27	2.0	0.65	0.92	7.60	4.48	440	—
C_2Cl_4, $\#F_1$	32	1.5	0.4	1.56	−15.0	433.2	156.9	4.0
C_2Cl_4, $\#F_2$	32	4.0	0.45	1.56	3.20	16.67	40.79	4.2
C_2Cl_4, $\#F_3$	32	1.5	0.55	1.03	−4.85	359.1	189.3	5.3
C_7H_8, $\#I\_0.3$	34	2.0	0.3	1.55	−7.784	7.79	2132.575	40
C_7H_8, $\#I\_0.35$	34	2.0	0.5	1.55	−1.19	78.9	2890.276	120
CCl_4, $\#F_1$	36	4.0	0.8	1.35	12.0	11.83	—	1.85
CCl_4, $\#F_2$	36	2.0	0.35	1.064	−4.37	10.58	—	1.58

it mostly does not experience the losses introduced by CCl_4. Although the confinement loss of fiber $\#F_1$ is always greater than that of $\#F_2$ in the whole wavelength range, it still has a higher nonlinear coefficient. So the larger confinement loss of $\#F_1$ in this case may not significantly affect the SC spectral broadening. However, the value of the fundamental mode at the pump pulse for $\#F_1$ fibers is 4.454 dB/m, much smaller than that of $\#F_2$ (19.406 dB/m), respectively. Table 1 presents the structure parameters and the characteristic quantities of proposed PCFs at the pump wavelength in comparison with some previous work on liquid-filled PCFs.

4. SC Generation in Proposed Fiber

The higher-order dispersion shows its important influence as the input pulse's center wavelength approaches ZDW and is computed through the development coefficients of the Taylor series around the center wavelength ω_0, the expansion of the propagation constant (ω) can be obtained by[49]

$$\beta(\omega) = \beta(\omega_0) + \beta_1(\omega_0)(\omega - \omega_0) + \frac{1}{2!}\beta_2(\omega_0)(\omega - \omega_0)^2 + \cdots . \tag{7}$$

Then the η_{th} order dispersion term can be calculated by taking the derivative of β concerning the angular frequency ω[20]

$$\beta_n = \left.\frac{d^n\beta}{d\omega^n}\right|_{\omega=\omega_0} . \tag{8}$$

The high-order dispersions at the pumping pulse frequency in our numerical modeling are displayed in Table 2.

Analysis of spectral formation through the impact of the dispersive and nonlinear processes of two proposed structures only for the fundamental mode is the aim of the next discussion. So, we simulated by numerically solving the generalized nonlinear

Table 2. The coefficient of high order dispersion at the pump wavelength.

Coefficients	$\#F_1$	$\#F_2$
β_2 (ps^2/m)	5.48×10^{-3}	-1.08×10^{-3}
β_3 (ps^3/m)	-1.17×10^{-5}	7.57×10^{-5}
β_4 (ps^4/m)	2.81×10^{-7}	-9.07×10^{-8}
β_5 (ps^5/m)	1.51×10^{-10}	4.44×10^{-10}
β_6 (ps^6/m)	1.68×10^{-12}	-3.73×10^{-12}
β_7 (ps^7/m)	-4.46×10^{-13}	9.88×10^{-15}
β_8 (ps^8/m)	6.37×10^{-16}	-1.52×10^{-16}
β_9 (ps^9/m)	1.62×10^{-16}	6.25×10^{-18}
β_{10} (ps^{10}/m)	-7.66×10^{-19}	5.83×10^{-20}
β_{11} (ps^{11}/m)	-4.89×10^{-20}	-3.05×10^{-21}

Schrödinger equation (GNLSE), based on the split-step Fourier method, which is given by the formula[49]:

$$\partial_z \tilde{A} - i\tilde{\beta}(\omega)\tilde{A} - \frac{\tilde{\alpha}(\omega)}{2}\tilde{A} = \mathrm{i}\gamma\left(1 + \frac{\omega - \omega_0}{\omega_0}\right)\tilde{A}\mathrm{F}\left[\int_{-\infty}^{\infty} R(T')|A|^2(T - T')dT'\right], \quad (9)$$

where $\tilde{A}(z, \omega)$ is the Fourier transform of the amplitude of a pulse $A(z, T)$, and $R(T')$ is the Raman response function. The left-hand side of Eq. (9) depicts the linear propagation effects of the fiber, $(\tilde{\alpha})$ and $(\tilde{\beta})$ are attenuation and dispersion in the frequency domain, respectively.

The pump wavelength is selected depending on the characteristic of the dispersion curve. Usually the pump wavelengths are chosen near the local maximum of the dispersion curve and close to the zero dispersion to find the expected small dispersion value. Therefore, for the two proposed fibers, the pump wavelengths selected will be different. The duration and energy related to the peak power of the input pulse strongly influence the broadening of the SC spectrum. Typically, the SC spectrum of fibers with anomalous dispersion properties will require higher peak power than those with all-normal dispersion. If the input peak power is too low, nonlinear effects are unlikely to occur, so the spectral expansion is negligible. However, the spectrum will also not broaden further if the peak power of the input pulse is too high, compared to other nonlinear properties of the fiber such as effective mode area and loss of the fibers. We can obtain SC radiation with the highest intensity and the broadest bandwidth by optimizing the intensity and wavelength of the pump.[51]

For $\#F_1$ and $\#F_2$ fibers, various nonlinear phenomena that appear during the SC simulation are typical for both all-normal and anomalous dispersions. There are two obvious advantages for us to use low energy pump pulses to obtain a broad SC spectrum in these simulations. Firstly, the nonlinear refractive index of CCl_4 is several times higher than that of fused silica (mentioned in Sec. 1). Second, the low effective area leads to the high nonlinearity of the two proposed fibers. In particular, the $\#F_1$ fiber generates a broad and flat-top SC spectrum with respect to the all-normal dispersion characteristics while $\#F_2$ gives a very broad and noisy SC

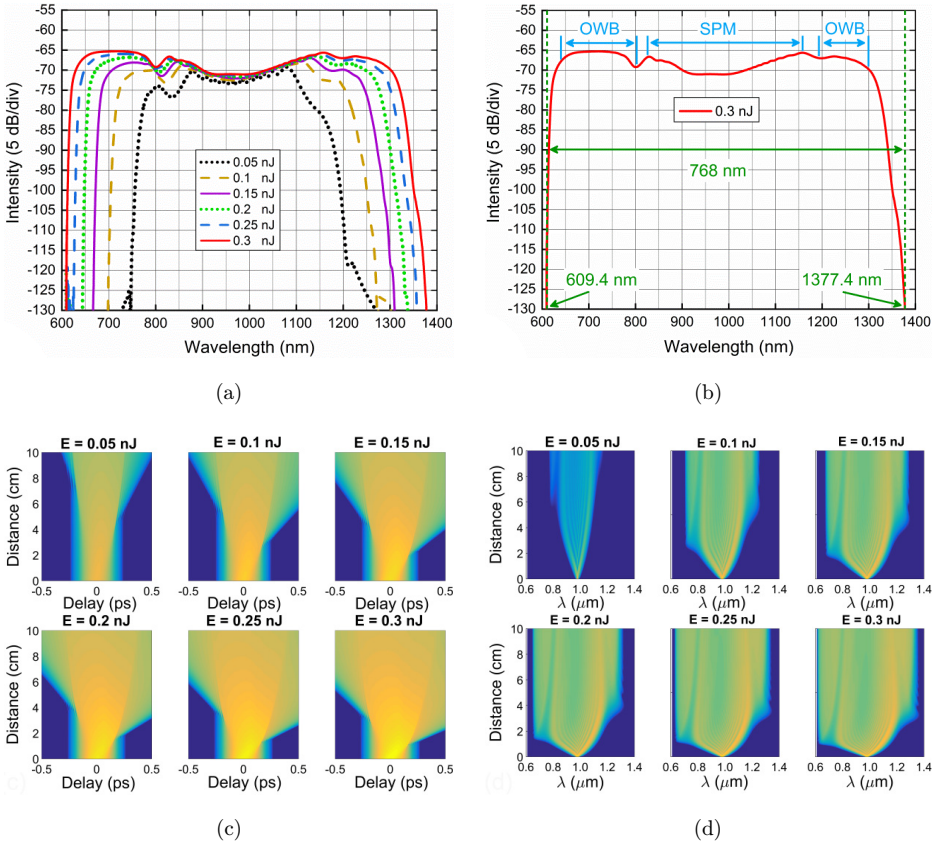

Fig. 7. For $\#F_1$ fiber: (a) the output spectrum for various input pulse energies when using pump pulses with 0.98 μm pump wavelength and 90 fs duration, (b) the output spectrum with the input pulse energy of 0.3 nJ, (c) the temporal profile at various propagation lengths, and (d) the spectral evolution of the SC along with fiber.

spectrum in the anomalous dispersion regime. Figure 7 depicts the pulse temporal and spectral evolution over the propagation distance. That is the result of launching a 90 fs pulse at an excitation wavelength of 0.98 μm into $\#F_1$ fiber with a propagation length of 10 cm. The spectral distributions of the optical pulses evolving along the infiltrated $\#F_1$ fiber with CCl_4 for an input energy range of 0.05–0.5 nJ are compared in Fig. 7(a). The spectrum is broadened as soon as the input pulse energy is as small as 0.05 and 0.1 nJ, which consists of many small peaks with the outermost peaks being the strongest. It is clear that by increasing the input energy, broader SC is achieved. When the input pulse energy is larger than 0.1 nJ, the small peaks also do not appear anymore, instead, the spectrum gets flatter and smoother, flat-top SC spectrum is obtained with the input energy reaching a maximum value of 0.3 nJ (Fig. 7(b)).

The dispersion, SPM, and OWB effects are mainly accountable for the process of the SC generation because the pump pulse works in the all-normal dispersion regime

of $\#F_1$ fiber. The OWB shows its influence on the shorter wavelength side even when the input pulse energy is very low (0.05 nJ), but the spectrum broadening is limited. When the input energy is greater than 0.05 nJ, SC process is initiated by SPM in the first few millimeters of propagation length causing the spectrum to broaden symmetrically towards both shorter and longer wavelengths. Later, the appearance of OWB at the wings of spectrum induced by four-wave mixing (FWM) leads to a strong asymmetry of the spectrum in both the blueshifted (trailing) edge of the pulse and the redshifted (leading) edge of the pulse. However, the increase in the effective mode area results in a decrease in the nonlinearity at longer wavelengths and allows the redshifted sideband to be strongly inhibited. More, spectral broadening towards the blue is also limited due to a steeper dispersion profile at shorter wavelengths although the higher input energy can be used to increase intensity at the trailing edge.[36,37,52] The output pulse has broadened to a range of 778 nm in the case of 0.3 nJ input pulse energy (Fig. 7(b)).

When the input energy is 0.3 nJ, the spectrum is broadened earlier towards the blue-side due to the onset of OWB which generates the new wavelengths around 800 nm at 1 cm propagation (Figs. 7(c) and 7(d)). During further propagation along the fiber, OWB occurs again at the red-side and the newly generated wavelengths around 1,200 nm appear at the distance of 3 cm of propagation. Next, the pulse spectrum continues to extend toward both sides, the group delay trace of the pulse is stretched out and the pulse spectrum becomes flatter on the wings. The SC spectra with flat-top is achieved covering the wavelength range of 609.4–1377.4 nm and benefits mainly from small and flat dispersion.

In this section, we investigate how anomalous dispersion can affect the SC generation of the $\#F_2$ fiber excited at 1.3 μm. An incident ultra-short pulses with 55 fs duration are injected into $\#F_2$ fiber propagating along 12 cm of fiber length shown in Fig. 8. The soliton dynamics such as SF, SSFS, and DW[18] plays a leading role when the ultra-short pulse propagates in $\#F_2$ fiber. So its SC spectrum is found to be much broader than that of the $\#F_1$ fiber, unfortunately the noise spectrum is more. The coherence of the SC is low due to the lack of coherence between the modulation instability frequency components and the pump. Furthermore, the fission of each soliton occurs randomly, so the fission products are completely incoherent.[27] As the input pulse propagates further, the Raman SSFS effect makes possible for the soliton components to move toward the low frequencies and the spectrum widens significantly towards the redshift wavelengths. Besides, the DW components are generated by the FWM process and propagate without any frequency shifting.[14]

Figures 8(a) and 8(b) denote the increase in spectral width with input pulse energy in the range 0.05–0.55 nJ. With a low input pulse energy (0.05 nJ), the spectrum SC has a long pulse width and narrow spectrum due to SPM. When the input energy is greater than 0.05 nJ, the soliton begins to appear and shows its role in the spectrum expansion but loses its symmetry structure as the pulse propagates at longer distances. The width of the spectrum increases gradually with increasing energy because of the appearance of new wavelength components. However, the

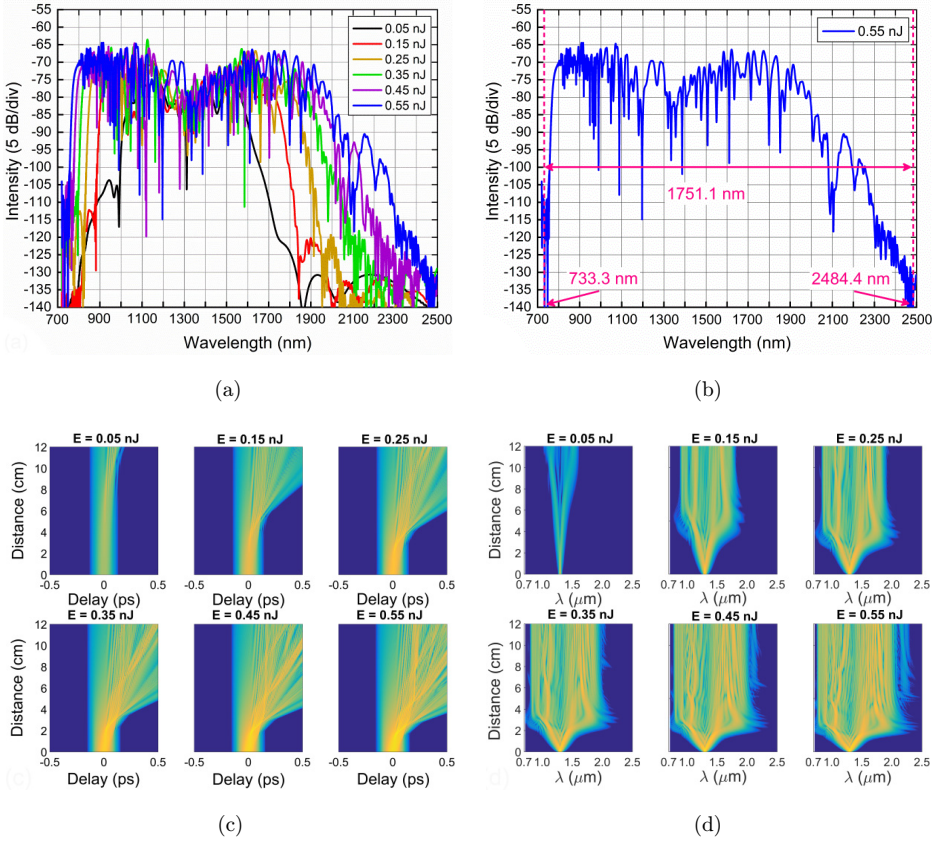

Fig. 8. For $\#F_2$ fiber: (a) the output spectrum for various input pulse energies when using pump pulses with 1.3 μm pump wavelength and 55 fs duration, (b) the output spectrum with the input pulse energy of 0.55 nJ, (c) the temporal profile at various propagation lengths, and (d) the spectral evolution of the SC along the fiber.

impact of the high steep dispersion in the short wavelengths range, low nonlinear coefficient, and high confinement loss in the long wavelength range restricts spectral broadening. Therefore, the spectral bandwidth hardly increases any more with further increase of input pulse energy (0.45 and 0.55 nJ). With a maximum value of 0.55 nJ of the input pulse energy, we obtain an SC spectrum spanning from 733.3 nm to 2484.4 nm. The temporal profile at various propagation lengths and the pulse evolution of the SC along with the fiber are denoted in Figs. 8(c) and 8(d). For an input pulse energy of 0.05 nJ, the ultra-short pulse experiences SPM during the first 1 cm, which compresses the pulse and broadens its symmetrical spectrum. When the input pulse approaches ZDW, the SF occurs at 2 cm of propagation length and a high order soliton begins to split into a series of fundamental solitons owing to higher order dispersion and Raman scattering.[22] Among all the fundamental solitons, the first fundamental soliton has the shortest duration and broad spectrum with the

Table 3. The SC bandwidth of proposed PCFs in comparison with other silica-based PCF infiltrations with liquid.

#	Refs.	T (fs)	E (nJ)	λ_p (μm)	Fiber length (cm)	SC range (nm)	Regime	Year
$\#F_1$	This work	90	0.3	0.98	10	768	all-normal	—
$\#F_2$	This work	55	0.55	1.3	12	1,751.1	anomalous	—
$CHCl_3$, $\#F_1$	27	400	1.0	1.03	10	660	all-normal	2019
$CHCl_3$, $\#F_2$	27	400	0.8	1.03	10	800	anomalous	2019
C_6H_6, $\#F_1$	29	90	3.0	1.56	1.0	1,300	all-normal	2021
C_6H_6, $\#F_3$	29	90	2.0	1.56	1.0	2,900	anomalous	2021
$C_6H_5NO_2$, $\#F_2$	30	90	0.5	1.56	5.0	1,300	all-normal	2020
$C_6H_5NO_2$, $\#F_3$	30	90	0.06	1.56	5.0	1,000	anomalous	2020
C_2Cl_4, $\#F_1$	32	90	1.5	1.56	5.0	1,200	all-normal	2021
C_2Cl_4, $\#F_2$	32	90	0.45	1.56	10	1,000	anomalous	2021
C_7H_8, #I_0.3	34	350	2.5	1.55	10	650	all-normal	2017
C_7H_8, #I_0.35	34	450	3.0	1.55	10	750	anomalous	2017
CCl_4	37	400	25	1.03	20	400	all-normal	2018

highest energy, which undergoes SSFS shift towards the red-side due to stimulated Raman scattering.[53] As a result, the spectrum moves towards the red-side, and the longer wavelengths move slower in the anomalous dispersion region,[54] the spectrum broadens to 2884.4 nm. Meanwhile, the blue-shifted DWs catch up with the first ejected soliton whose speed is reduced due to the high dispersion slope. This interaction generates new wavelength components through FWM effect, which broadens the deep blue region of the spectrum to 733.3 nm.

Results from the above simulation analyses show that nonlinear effects play an important role in the SC generation process which is often dominated by the dispersion and nonlinear properties of PCFs. The highly nonlinearity of CCl4 and reasonable structural modification are also key factors that enable the PCF to generate much broadened spectrum with low input energy and within short propagating distance. We achieve a broader SC spectrum for both all-normal and anomalous dispersions in comparison with other liquid-filled PCFs (Table 3).

5. Conclusion

The CCl_4-filled PCF with the diversity of dispersion was designed by adjusting the diameters d_1 and d_2 of the first ring near the core and the others in the cladding of PCF to obtain a flat and small dispersion. Two fibers with reasonable dispersion, high nonlinear coefficient, and low confinement loss are introduced to investigate in detail the SC generation process. With lattice constant $\Lambda = 1.0\,\mu$m and filling factor $d_1/\Lambda = 0.6$, $\#F_1$ fiber has the anomalous dispersion regime, generates a flat-top and smooth SC via SPM effect followed by OWB. It is easy to achieve 768 nm bandwidth with low input pulse energy of 0.3 nJ at a pump wavelength of 0.98 μm. $\#F_2$ fiber ($\Lambda = 2.0\,\mu$m and $d_1/\Lambda = 0.3$) generates a broad SC with a spectral bandwidth of 1,751.1 nm within 5 dB. The soliton dynamics is the major contributor to the SC

process because this fiber is pumped in an anomalous dispersion regime with a pump wavelength of 1.3 μm and a low input pulse energy of 0.55 nJ. The designed PCF, can be a new class of fibers for the next generation of a broadband source.

References

1. Y. Shen, A. A. Voronin, A. M. Zheltikov, S. P. O'Connor, V. V. Yakovlev, A. V. Sokolov and M. O. Scully, Supercontinuum generation in large-mode-area photonic crystal fbers for coherent Raman microspectroscopy, in *Proc. SPIE 10522, Frontiers in Ultrafast Optics: Biomedical, Scientific, and Industrial Applications XVIII* (2018), p. 105220I. doi: 10.1117/12.2285103.
2. H. Pakarzadeh, R. Derakhshan and S. Hosseinabadi, Tunable wavelength conversion based on optofluidic infiltrated photonic crystal fibers, *J. Nonlinear Opt. Phys. Mater.* **28**(1) (2019) 1950002. doi: 10.1142/S0218863519500024.
3. M. Yamanaka, H. Kawagoe and N. Nishizawa, High-power supercontinuum generation using high-repetition-rate ultrashort-pulse fiber laser for ultrahigh-resolution optical coherence tomography in 1600 nm spectral band, *Appl. Phys. Express* **9**(2) (2016) 022701. doi: 10.7567/APEX.9.022701.
4. S. Sharma and J. Kumar, Numerical analysis of optical logic gate based on nonlinear optical loop mirror with a photonic crystal fiber, *J. Nonlinear Opt. Phys. Mater.* **24**(2) (2015) 1550019. doi: 10.1142/S0218863515500198.
5. S. Dupont, C. Petersen, J. Thøgersen, C. Agger, O. Bang and S. R. Keiding, IR microscopy utilizing intense supercontinuum light source, *Opt. Express* **20**(5) (2012) 4887–4892. doi: 10.1364/OE.20.004887.
6. Z. Dashtban, M. R. Salehi and E. Abiri, Supercontinuum generation in near-and mid-infrared spectral region using highly nonlinear silicon-core photonic crystal fiber for sensing applications, *Photon. Nanostruct.–Fundam. Appl.* **46** (2021) 100942. doi: 10.1016/j.photonics.2021.100942.
7. N. Nishizawa, Generation and application of high-quality supercontinuum sources, *Opt. Fiber Technol.* **18**(5) (2012) 394–402, doi: 10.1016/j.yofte.2012.06.010.
8. H. Pakarzadeh, M. Taghizadeh and M. Hatami, Designing a photonic crystal fiber for an ultra-broadband parametric amplification in telecommunication region, *J. Nonlinear Opt. Phys. Mater.* **25**(2) (2016) 1650023. doi: 10.1142/S0218863516500235.
9. C. Cheng, Y. Ou, J. Zhang, Q. Lv, J. Zhu and H. Lv, Design of all-normal dispersion photonic crystal fiber for high coherent broadband supercontinuum generation in the telecommunication window, *J. Nonlinear Opt. Phys. Mater.* **24**(3) (2015) 1550026. doi: 10.1142/S0218863515500265.
10. Y. J. You, C. Wang, Y. L. Lin, A. Zaytsev, P. Xue and C. L. Pan, Ultrahigh-resolution optical coherence tomography at 1.3 μm central wavelength by using a supercontinuum source pumped by noise-like pulses, *Laser Phys. Lett.* **13**(2) (2016) 025101. doi: 10.1088/1612-2011/13/2/025101.
11. A. Labruyère, A. Tonello, V. Couderc, G. Huss and P. Leproux, Compact supercontinuum sources and their biomedical applications, *Opt. Fiber Technol.* **18**(5) (2012) 375–378. doi: 10.1016/j.yofte.2012.08.003.
12. B. Schenkel, R. Paschotta and U. Kelle, Pulse compression with supercontinuum generation in microstructure fibers, *J. Opt. Soc. Am. B* **22**(3) (2005) 687–693. doi: 10.1364/JOSAB.22.000687.
13. K. Saitoh, N. J. Florous and M. Koshiba, Theoretical realization of holey fiber with flat chromatic dispersion and large mode area: An intriguing defected approach, *Opt. Lett.* **31**(1) (2006) 26–28. doi: 10.1364/OL.31.000026.

14. M. Z. Alam, M. I. Tahmid, S. T. Mouna, M. A. Islam and M. S. Alam, Design of a novel star type photonic crystal fiber for mid-infrared supercontinuum generation, *Opt. Commun.* **500** (2021) 127322, https:doi:10.1016/j.optcom.2021.127322.
15. J. C. Knight, Photonic crystal fibers, *Nature* **424** (2003) 847–851. doi: 10.1038/nature01940.
16. D. M. B. Lesko, H. Timmers, S. Xing, A. Kowligy, A. J. Lind and S. A. Diddams, A six-octave optical frequency comb from a scalable few-cycle erbium fibre laser, *Nat. Photonics* **15** (2021) 281–286. doi: 10.1038/s41566-021-00778-y.
17. U. Elu, L. Maidment, L. Vamos, F. Tani, D. Novoa, M. H. Frosz, V. Badikov, D. Badikov, V. Petrov, P. St. J. Russell and J. Biegert, Seven-octave high-brightness and carrier-envelope-phase-stable light source, *Nat. Photonics* **15** (2021) 277–280. doi: 10.1038/s41566-020-00735-1.
18. P. P. Ho and R. R. Alfano, Optical Kerr effect in liquids, *Phys. Rev. A* **20**(5) (1979) 2170–2187. doi: 10.1103/PhysRevA.20.2170.
19. C. J. Pouchert, *The Aldrich Library of Infrared Spectra*, 3rd edn. (Aldrich Chemical., 1981).
20. R. Raei, M. E. Heidari and H. Saghaei, Supercontinuum generation in organic liquid-liquid core-cladding photonic crystal fiber in visible and near-infrared regions, *J. Opt. Soc. Am. B* **35**(2) (2018) 323–330. doi: 10.1364/josab.35.000323.
21. J. Challenor, *Toxicology of Solvents* (Rapra Technology, 2002). doi: 10.1093/occmed/52.6.363-a.
22. J. M. Dudley and J. R. Taylor, *Supercontinuum Generation in Optical Fibers* (Cambridge University Press, 2010). doi: 10.1017/CBO9780511750465.
23. J. M. Dudley, Coherence properties of supercontinuum spectra generated in photonic crystal and tapered optical fibers, *Opt. Lett.* **27**(13) (2002) 1180–1182. doi: 10.1364/OL.27.001180.
24. Y. Fang, C. Bao, Z. Wang, B. Liu, L. Zhang, X. Han, Y. He, H. Huang, Y. Ren, Z. Pan and Y. Yue, Three-octave supercontinuum generation using SiO_2 cladded Si_3N_4 slot waveguide with all-normal dispersion, *J. Lightw. Technol.* **38**(13) (2020) 3431–3438. doi: 10.1109/JLT.2020.2985262.
25. C. Finot, B. Kibler, L. Provost and S. Wabnitz, Beneficial impact of wave-breaking for coherent continuum formation in normally dispersive nonlinear fibers, *J. Opt. Soc. Am. B* **25**(11) (2008) 1938–1337. doi: 10.1364/JOSAB.25.001938.
26. M. F. S. Ferreira, *Optical Signal Processing in Highly Nonlinear Fibers*, 1st edn. (CRC Press, 2020). doi: 10.1201/9780429262111.
27. L. C. Van, V. T. Hoang, V. C. Long, K. Borzycki, K. D. Xuan, V. T. Quoc, M. Trippenbach, R. Buczyński and J. Pniewski, Optimization of optical properties of photonic crystal fibers infiltrated with chloroform for supercontinuum generation, *Laser Phys.* **29**(7) (2019) 075107-9. doi: 10.1088/1555-6611/ab2115.
28. R. Ahmad, M. Komanec and S. Zvanovec, Ultra-wideband mid-infrared supercontinuum generation in liquid-filled circular photonic crystal fiber, *J. Nanophoton.* **14**(2) (2020) 026016. doi: 10.1117/1.JNP.14.026016.
29. L. C. Van, V. T. Hoang, V. C. Long, K. Borzycki, K. D. Xuan, V. T. Quoc, M. Trippenbach, R. Buczyński and J. Pniewski, Supercontinuum generation in benzene-filled hollow-core fibers, *Opt. Eng.* **60**(11) (2021) 116109. doi: 10.1117/1.OE.60.11.116109.
30. L. C. Van, V. T. Hoang, V. C. Long, K. Borzycki, K. D. Xuan, V. T. Quoc, M. Trippenbach, R. Buczyński and J. Pniewski, Supercontinuum generation in photonic crystal fibers infiltrated with nitrobenzene, *Laser Phys.* **30**(3) (2020) 035105. doi: 10.1088/1555-6611/ab6f09.

31. Y. Guo, J. H. Yuan and K. Wang, Generation of supercontinuum and frequency comb in a nitrobenzene-core photonic crystal fiber with all-normal dispersion profile, *Opt. Commun.* **481**(4) (2021) 126555. doi: 10.1016/j.optcom.2020.126555.
32. H. V. Le, V. T. Hoang, H. T. Nguyen, V. C. Long, R. Buczynski and R. Kasztelanic, Supercontinuum generation in photonic crystal fibers infiltrated with tetrachloroethylen, *Opt. Quantum Electron.* **53** (2021) 187–205. doi: 10.1007/s11082-021-02820-3.
33. V. T. Hoang, R. Kasztelanic, A. Anuszkiewicz, G. Stepniewski, A. Filipkowski, S. Ertman, D. Pysz, T. Wolinski, K. D. Xuan, M. Klimczak and R. Buczynski, All-normal dispersion supercontinuum generation in photonic crystal fibers with large hollow cores infiltrated with toluene, *Opt. Mater. Express* **8**(11) (2018) 3568–3582. doi: org/10.1364/OME.8.003568.
34. L. C. Van, A. Anuszkiewicz, A. Ramaniuk, R. Kasztelanic, K. D. Xuan, V. C. Long, M. Trippenbach and R. Buczyński, Supercontinuum generation in photonic crystal fibres with core filled with toluene, *J. Opt.* **19**(12) (2017) 125604. doi: 10.1088/2040-8986/aa96bc.
35. T. N. Thi, D. H. Trong, B. T. Le Tran, T. D. Van and L. C. Van, Optimization of optical properties of toluene-core photonic crystal fibers with circle lattice for supercontinuum generation, *J. Opt.* (2022). doi: 10.1007/s12596-021-00802-y.
36. Q. H. Dinh, J. Pniewski, H. L. Van, A. Ramaniuk, V. C. Long, K. Borzycki, D. X. Khoa, M. Klimczak and R. Buczyński, Optimization of optical properties of photonic crystal fibers infiltrated with carbon tetrachloride for supercontinuum generation with subnanojoule femtosecond pulses, *Appl. Opt.* **57**(14) (2018) 3738–3746. doi: 10.1364/ao.57.003738.
37. V. T. Hoang, R. Kasztelanic, A. Filipkowski, G. Stępniewski, D. Pysz, M. Klimczak, S. Ertman, V. C. Long, T. R. Woliński, M. Trippenbach, K. D. Xuan, M. Śmietana and R. Buczyński, Supercontinuum generation in an all-normal dispersion large core photonic crystal fiber infiltrated with carbon tetrachloride, *Opt. Mater. Express* **9**(5) (2019) 2264–2278. doi: 10.1364/OME.9.002264.
38. V. T. Hoang, R. Kasztelanic, G. Stępniewski, K. D. Xuan, V. C. Long, M. Trippenbach, M. Klimczak, R. Buczyński and J. Pniewski, Femtosecond supercontinuum generation around 1560 nm in hollow-core photonic crystal fibers filled with carbon tetrachloride, *Appl. Opt.* **59**(12) (2020) 3720–3725, doi: 10.1364/AO.385003.
39. H. V. Le, V. T. Hoang, G. Stępniewski, T. Le Canh, N. Vo Thi Minh, R. Kasztelanic, M. Klimczak, J. Pniewski, K. X. Dinh, A. M. Heidt and R. Buczyński, Low pump power coherent supercontinuum generation in heavy metal oxide solid-core photonic crystal fibers infiltrated with carbon tetrachloride covering 930–2500 nm, *Opt. Express* **29**(24) (2021) 39586–39600. doi: 10.1364/OE.443666.
40. A. Medjouri, L. M. Simohamed, O. Ziane, A. Boudrioua and Z. Becer, Design of a circular photonic crystal fiber with flattened chromatic dispersion using a defected core and selectively reduced air holes: Application to supercontinuum generation at 1.55 μm, *Sci. Direct Photonics Nanostruct. Fundam Appl.* **16** (2015) 43–50. doi: 10.1016/j.photonics.2015.08.004.
41. T. Huang, P. Huang, Z. Cheng, J. Liao, X. Wu and J. Pan, Design and analysis of a hexagonal tellurite photonic crystal fiber with broadband ultra-flattened dispersion in mid-IR, *Optik* **167** (2018) 144–149. doi: 10.1016/j.ijleo.2018.04.016.
42. M. Vieweg, S. Pricking, T. Gissibl, Y. Kartashov, L. Torner and H. Giessen, Tunable ultrafast nonlinear optofluidiccoupler, *Optics Letters.* **37**(6) (2012) 1058–1060. https://doi.org/10.1364/OL.37.001058.
43. J. Meister, R. Franzen, G. Eyrich, J. Bongartz, N. Gutknecht and P. Hering, First clinical application of a liquid-corelight guide connected to an Er: YAG laser for oral treatment of leukoplakia, *Lasers Med. Sci.* **25**(5) (2010) 669–673. doi: 10.1007/s10103-010-0782-0.

44. K. Moutzouris, M. Papamichael, S. C. Betsis, I. Stavrakas, G. Hloupis and D. Triantis, Refractive, dispersive and thermo-optic properties of twelve organic solvents in the visible and near-infrared, *Appl. Phys. B* **116**(3) (2013) 617-622. doi: 10.1007/s00340-013-5744-3.
45. C. Z. Tan, Determination of refractive index of silica glass for infrared wavelengths by IR spectroscopy, *J. Non-Cryst. Solids* **223**(1–2) (1998) 158–163. doi: 10.1016/s0022-3093(97)00438-9.
46. I. Kubat and O. Bang, *Opt. Express* **24**(3) (2016) 2513–2526. doi: 10.1364/OE.24.002513.
47. Y. S. Lee, C. G. Lee, F. Bahloul, S. Kim and K. Oh, Simultaneously achieving a large negative dispersion and a high birefringence over Er and Tm dual gain bands in a square lattice photonic crystal fiber, *J. Lightw. Technol.* **37**(4) (2019) 1254–1263. doi: 10.1109/JLT.2019.2891756.
48. F. Begum, Y. Namihira, T. Kinjo and S. Kaijage, Supercontinuum generation in square photonic crystal fiber with nearly zero ultra-flattened chromatic dispersion and fabrication tolerance analysis, *Opt. Commun.* **284**(4) (2011) 965–970. doi: 10.1016/j.optcom.2010.10.029.
49. G. P. Agrawal, *Nonlinear Fiber Optics*, 5th edn., Chap. 2 (Academic Press, Elsevier, 2013). doi: 10.1016/C2011-0-00045-5.
50. C. Wei, H. Zhang, H. L. Hongxi and S. Y. Liu, Broadband mid-infrared supercontinuum generation using a novel selectively air-hole filled As_2S_5-As_2S_3 hybrid PCF, *Optik* **141** (2017) 32–38. doi: 10.1016/j.ijleo.2017.02.061.
51. H. Lei, J. Yao, J. Zhao, H. Xie, F. Zhang, H. Zhang, N. Zhang, G. Li, Q. Zhang, X. Wang, Y. Yang, L. Yuan, Y. Cheng and Z. Zhao, Ultraviolet supercontinuum generation driven by ionic coherence in a strong laser field, *Nat. Commun.* **13** (2022) 4080. doi: 10.1038/s41467-022-31824-0.
52. A. Medjouria and D. Abed, Design and modelling of all-normal dispersion $As_{39}Se_{61}$ chalcogenide photonic crystal fiber for flat-top coherent mid-infrared supercontinuum generation, *Opt. Fiber Technol.* **50** (2019) 154–164. doi: 10.1016/j.yofte.2019.03.021.
53. Y. Huang, H. Yang, S. Zhao, Y. Mao and S. Chen, Design of photonic crystal fibers with flat dispersion and three zero dispersion wavelengths for coherent supercontinuum generation in both normal and anomalous regions, *Results Phys.* **23** (2021) 104033. doi: 10.1016/j.rinp.2021.104033.
54. S. Roy, D. Ghosh, S. K. Bhadra and G. P. Agrawal, Role of dispersion profile in controlling emission of dispersive waves by solitons in supercontinuum generation, *Opt. Commun.* **283**(15) (2010) 3081–3088. doi: 10.1016/j.optcom.2010.04.003.